Space Charge Compensation of Negative Ion Beams

M. Cavenago*[1], P. Veltri[2]
[2]INFN/LNL, Laboratori Nazionali di Legnaro, [2]Consorzio RFX, Assoc. Euratom-ENEA sulla Fusione
* viale dell'Universita' n. 2, I-35020 Legnaro (PD) Italy, cavenago@lnl.infn.it

Abstract: The transport of intense ion beams with reduced beam divergence over reasonable drift distances requires a reliable compensation of the beam space charge. In the case of negative ion beams (required in the Neutral Beam Injectors envisioned for the ITER tokamak) this background charge is provided by the accumulation of positive slow ions (mainly H_2^+) produced by ionization of the residual gas in the drift tube, via the reaction: $H^- + H_2 \rightarrow H^{x-} + H_2^+ + (2-x)e$ (with $x = 0, 1$). Primary beam currents is about 300 A/m2, so that Poisson equation has a nonlinear space charge density due to particles. In a flexible set of macros called BYPO previously developed, suitable for running under Comsol Multiphysics, the positive ion background was represented by a semi empirical model, reaching 100% space charge compensation at beam core. Here a 2D selfconsistent diffusive model of the background is introduced, implemented in Comsol Multiphysics and solved, discussing also its relation with more complex hydrodynamics models and the previous 1D models. Using postprocessing routines, the production of H_2^+ and other secondaries is also separately computed, finding a background positive charge roughly in agreement with this model.

Keywords: ion beams, secondary beam

1 Introduction

The propagation of a high charge ion beam (despite its space charge) inside accelerator is made possible by the curvature of the accelerating field equipotentials, so that electrodes should be carefully designed [1, 2, 3]. In the region after the accelerator exit, called the drift region, the so-called space charge compensation (SCC) (due to accumulation of secondary particles that are slow ions and/or electrons formed by collisions of the ion beam with gas) greatly helps the propagation of beam [4]. In most simulation codes, this is simply modeled imposing a fixed ratio R^{sc} of the secondary density respect to primary beam density $N_b(\mathbf{x})$. Analytical studies, based only on a 1D radial model, does indeed forecast a large compensation fraction, say $R^{sc} = 1.00$ negative H^- ion beams and $R^{sc} \cong 0.98$ for H^+ ions at typical speed $v_b = 4.4 \times 10^6$ m/s, average beam density $N_0 = 5.6 \times 10^{14}$ m^{-3}, beam radius $b = 6$ mm and gas pressure $p_g = 0.05$ Pa. In this paper we address the axial flow of secondary ion with two Comsol Multiphysics models; this flow may modify locally R^{sc} and can consequently slightly perturb the primary beam propagation (section 2 and 3).

Some Monte Carlo simulations with electrostatic fields computed by Comsol Multiphysics here presented in section 4 shows significant fluctuations of the SCC. Finally in section 5 we recall the ad hoc model of SCC used in BYPO[2, 3] for comparison. In the literature both radial transport 1D codes [1] and Monte Carlo codes [5] are well documented for positive ions. Experimental effects of SCC were also discussed[6].

For negative ions, we can consider only two major collision process, called background ion ionization and primary beam stripping

$$\underline{H}^- + H_2 \rightarrow \underline{H}^- + e + H_2^+ \qquad (1)$$

$$\underline{H}^- + H_2 \rightarrow \underline{H}^0 + \underline{e} + H_2 \qquad (2)$$

where we mark with an underline the fast particles that approximately maintains the v_b speed. We may have the sum of these two processes in one collision. The effective collision cross section are about $\sigma_1 = 2 \times 10^{-20}$ m^{-2} and $\sigma_2 = 3 \times 10^{-20}$ m^{-2} (for 100 keV H^-) [7]. In eq. 2 electrons have about 60 eV energy, while in eq. 1 they get 10 eV energy and H_2^+ speed is not much greater than the gas one.

A scheme of a typical experimental situation is given in fig 1 and 2; here we take a 2D section and show two beamlets for illustration (a vertical section of the ITER accelerator will show 80 beamlets, while the minimum beamlet number is of course one). Inside accelerator, electrodes (with grids of holes) are closer to beamlets, so they shield any other electrode; but in the large open spaces of the drift region, the potential V_D of the so-called drift tube enclosing the beamlets is important. Here by convention the drift tube is the ground, so $V_D = 0$ and the potential V_{PA}) of the last electrode PA is to be optimized. Precisely speaking, in a 2D zx-geometry holes and tubes become channels, with a height of 1 meter in y-direction; for example $2R_t$ is the width of the drift channel.

Before the PA we have a strong electric field $E_z < 0$; this field imbues the PA holes and attracts H_2^+ back to the accelerator, spoiling the SCC for quite a distance; to mitigate this, we are ready to bias V_{PA} from +200 V, to repel H_2^+ inside the drift region. If this is not enough, we can add a repeller electrode REP after the PA.

In the experience with negative ion beam (40 mA per beamlet as planned for ITER) the SCC was generally found satisfying enough even without PA biasing[8, 9, 10]. On the other side, repeller electrodes are usually added at both ends of the drift tube for intense positive ion beam (130 mA as planned for example for IFMIF [5]) due the greater beam quality there required.

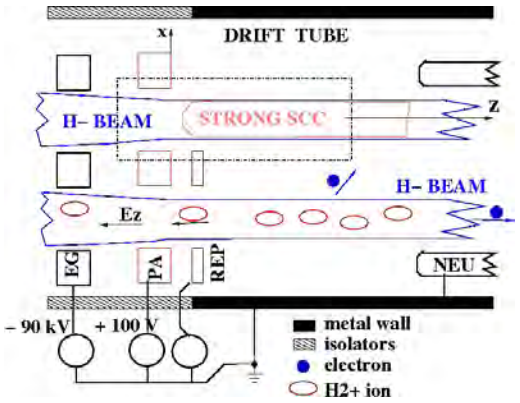

Figure 1: A scheme of the accelerator end section. In lower beam, some particle positions and velocities are put into evidence; NEU is for neutralizer. Simulation region (dashed border rectangle) is expanded in fig. 2.

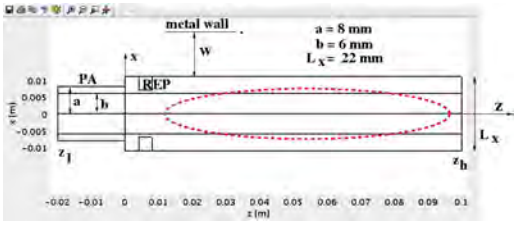

Figure 2: Simulation geometry

2 Basic equation and simplification

Introducing a reference temperature $T_0 = 1$ eV, we can determine a Debye length $\lambda_D = (\epsilon_0 T/e^2 N_0)^{1/2}$ where N_0 is the average beam density, and a sound speed $c_s = (T_0/m_{H_2^+})^{1/2}$. With the scaled density $n_i = N_i/N_0$ and the potential $u = -e\phi/T_0$ the Poisson equation becomes

$$\lambda_D^2 \triangle u = n_2 - n_e - n_b \equiv n_a \qquad (3)$$

with the shorthand $n_2 = n_{H_2^+}$ and $n_b = n_{H^-}$.

We may assume that beam is parallel exiting PA and, for a short simulation region as shown in fig. 1 and 2, the propagating beam has no time to diverge; also we keep beam speed v_b fixed in first approximation. So we use a fixed beam density, as a flat beam profile $n_b = \Theta(b - |x|)$ or a parabolic profile $n_b = 1.5 \max(0, 1 - (x/b)^2)$.

In this first model electron density is neglected both for simplicity and for the following justifications. For the greater thermal speed of electron, n_e is expect to be order of one % of n_2. Even if the electron density is known to be important for instability suppression[6], if a stationary model would prove that H_2^+ may accumulate to compensate n_b fully, it is reasonable to expect that also $n_b + n_e$ can be similarly compensated.

The slow ion conservation equation is

$$\mathrm{div}(n_2 \mathbf{v}) = n_b/\lambda_g \qquad (4)$$

where $\mathbf{v}$ is the average ion velocity (divided by c_s) and $\lambda_g = c_s/(N_g \sigma_1 v_b)$ is reference length typical of SCC; here $N_g = 1.2 \times 10^{19}$ m^3 the gas density. The momentum conservation takes the form

$$\mu(\mathbf{v}\cdot\nabla)\mathbf{v} = \nabla u - \frac{\nabla p}{n_2 T_0} - \frac{\mathbf{v}}{\lambda_2} + R_c - \frac{n_b \mathbf{v}}{n_2 \lambda_g} \qquad (5)$$

where $\mu = 1$ to maintain the convective term, p is the pressure, λ_2 is the mean free

path, determined from (nearly) elastic collisions of H_2^+ with other particles, and R_c are the other effects (if any) of those collisions; the last term expresses the fact that ions are produced by eq 1 at rest and this decreases the average speed [11]. It should be noted that this continuous generation of ions spreads the distribution of velocities (still different from a maxwellian); [so a free-fall model would be a possible choice, but it seems affordable in 1D radial calculations at most [1]]. Moreover this spread is the origin of the pressure p, given by a separated balance equation in principle. Here we close the equations by assuming $p = n_2 T_0$..

The mean free path estimate λ_2 also includes the reaction

$$H_2^+ + H_2 \rightarrow H^0 + H_3^+ \tag{6}$$

since a H_3^+ will be transported similarly to a H_2^+ ion; its cross section is $\sigma_3 = 1.9 \times 10^{-19}$ m^2 at $T_0 = 1$ eV. In comparison the elastic cross section is $\sigma_4 = 1.3 \times 10^{-19}$ m^2 [12]. The Coulomb collisions between H^- primary were studied too, also because they may heat the ions; both collision rate and heat transfer rate (computed with the classical theory [13]) are anyway fully negligible

2.1 The diffusion model

It can be argued that, when the beam space charge is fully neutralized, the electric field is small and slowly changing inside in the core of the drift region space (the dashed ellipse in fig 2) so that $\mathbf{v}$ is small and the convective term can be dropped in eq. 5. Formally this amount to put $\mu = 0$; after defining an effective free path λ_e we solve for $\mathbf{v}$ as

$$\lambda_e^{-1} = \lambda_2^{-1} + (n_b/n_2\lambda_g) \tag{7}$$

$$\mathbf{v} = \lambda_e \nabla(u - \log n_2) \tag{8}$$

Substituting this in eq. 4, we get the

$$\mathrm{div}\{\lambda_e n_2(\nabla u) - \lambda_e(\nabla n_2)\} = n_b/\lambda_g \tag{9}$$

where inside the divergence operator we recognize the usual current given by the Fick's law (mobility+diffusion terms).

2.2 Boundary condition (bc)

Our simulation region has a very limited extension in x direction: $|x| \leq L_x/2$, where L_x is the spacing of the holes in a multiaperture electrodes; in other words, our simulation domain is the region common both to a single beamlet system and a many beamlet system. By a proper choice of bc at lower and upper boundaries we can approximately simulate both systems, also economizing problem memory size. For the single beamlet case, we know that there is a wall with $u = 0$ at a distance $w = R_t - 0.5L_x$ (in planar geometry) from our boundary; by a series expansion in w we approximate u at wall with $u + w\mathbf{n} \cdot \nabla u$ at boundary, and set this value to zero; here $\mathbf{n}$ is the outward normal. Introducing $i_w = 1/w$ we finally write

$$\mathbf{n} \cdot \nabla u = -i_w u \quad \text{at} \quad x = \tfrac{1}{2}L_x \tag{10}$$

For the case of an infinite array of beamlets, we have symmetry at upper and lower boundaries, so that bc is eq 10 with $i_w = 0$. At the exit plane $z = z_h$ (in the middle of an open space like the drift tube) we assume again a simple Neumann condition. Of course at the PA we have a fixed potential $u = u_{PA}$. At the beam input plane $z = z_l$ we can assume that $u_{,z}(z_l, x)$ is known by simulations on larger scales. In particular, if we imagine that the PA hole extends even for $z < z_l$ or that z_l is in the middle of the PA hole, we conclude that beam space charge is symmetric around z_l and does not contribute to $u_{,z}$, the z-derivative of u. The lower mode of the remaining Laplace equation is $u = c_1 \exp(-k_0 z)\cos(k_0 x)$ with c_1 a constant and $k_0 = \pi/(2a)$ where $2a$ is the entrance channel width. In summary

$$u_{,z}(z_l, x) = u_1 \cos(k_0 x) \tag{11}$$

where u_1 is a parameter assigned by the user. The condition for density n_2 approximately follows from considering $\lambda_e n_2 \nabla u$ as a convective flow (and $-\lambda_e \nabla n_2$ as the diffusive flow). When ions hits the PA, they immediately become neutral, so no ion can diffuse back: convective flow has no restriction and diffusive flow is zero, that is

$$\mathbf{n} \cdot \nabla n_2 = 0 \tag{12}$$

At the exit plane, $n_{2,z} = 0$ if we want to obtain an equilibrium, so we can still impose eq. 12. Finally at the upper and lower boundary we can have a partial recirculation of ions from one beamlet to another: precisely assume that a fraction R_c of the ions

that exit (if any) diffuses back. So

$$\mathbf{n} \cdot \nabla n_2 = \max(0, R_c n_2 \mathbf{n} \cdot \nabla u) \qquad (13)$$

Even in the many beamlet case we guess $R_c \leq 0.5$. It is indeed not realistic to take $R_c = 1$ since ions escaping from one beamlet may as well pass through beamlets and arrive to the drift tube wall. In the case of a single beamlet the recirculation fraction R_c is zero, so that eq. 13 becomes eq. 12.

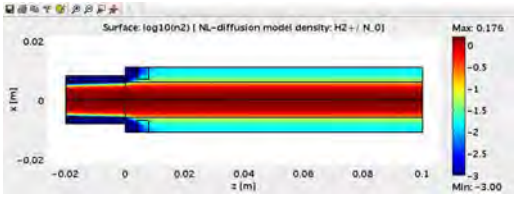

Figure 3: Map of the normalized ion density n_2, to enhance graph visibility, we plot the decimal log, with a minimum displayed n2 of 0.001

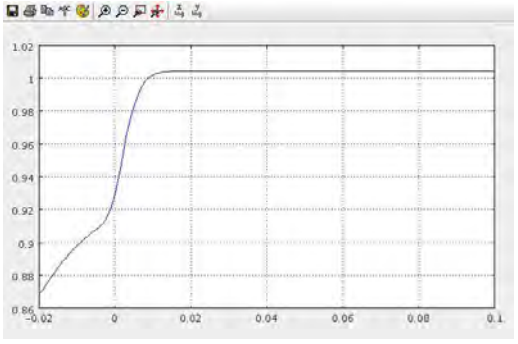

Figure 4: Plot of $\int \mathrm{d}x\, n_2(z,x) / \int n_b$

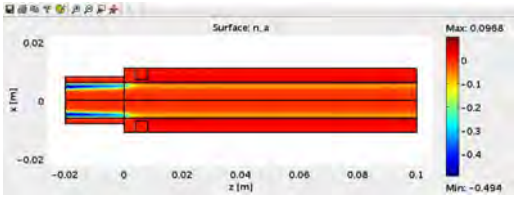

Figure 5: Map of the normalized charge n_a

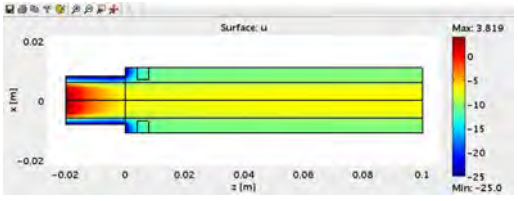

Figure 6: Map of the normalized potential u

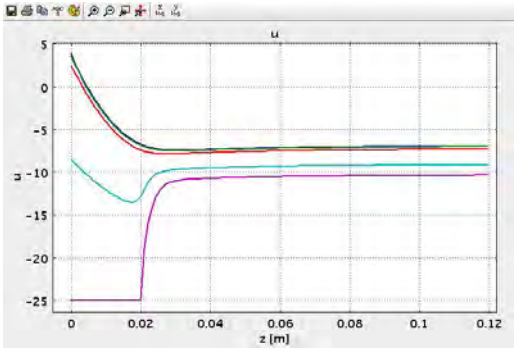

Figure 7: The normalized potential $u(z,x)$ for $x = 0, 2, 4, 6$ and 8 mm; the first two lines are superposed (green); the last line (magenta) touch the PA visibly

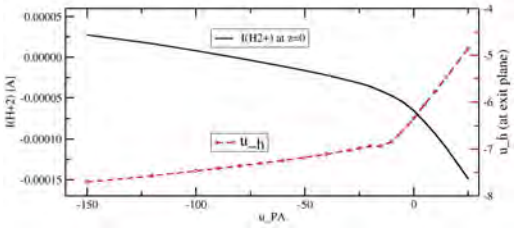

Figure 8: Plots of end potential $u_h = u(z_h, 0)$ vs PA potential u_{PA}; also shown current of H_2^+ crossing $z = 0$ plane (y extension= 1m).

3 Results

It is well known that eqs. 3-5 system is not suitable for nonlinear solvers, unless proper stabilization schemes are adopted [14, 15]. So we thus use the reduced system of eqs. 3 and 9 for a preliminary modelling (with $n_2 = 1$ in eq. 7). Here we restrict to the single beamlet case, so $R_c = 0$ and we take $i_w = 25$ m^{-1} (corresponding to drift channel width of 102 mm). Other dimensions are given in fig 2. We set $u_{PA} = -25$ and a modest field inside PA: $u_1 = 10^3/$ m.

The more novel result noted is the distribution of H_2^+ ions shown in Fig 3. A cloud of H_2^+ ions extends also outside the beam. To obtain a nearly zero potential $u(z,0)$ from eq. 3 is necessary that the total charge n_a integrated on all x is near to zero, and indeed we see this compensation in fig 4. The existence of H_2^+ outside the beam so implies that inside the beam, especially near borders, we have a local space charge compensation less than 100 % (see the yellow lines in fig 5).

Potential u is shown in figs 6 and 7; in this case axial compensation settles very

rapidly, so the only regions where we find a large electric field is the PA hole; there we found the largest unbalance of the total space charge n_a (see fig 5, according to Poisson equation. It is interesting to plot the net current of H_2^+ (exiting from or falling inside the PA channel, at $z = 0$) and the end axis potential $u_h = u(z_h, 0)$ against the u_{PA}; see in Fig 8: For the modest u_1, any $u_P A \leq -20$ V suffices to keep back streaming under 30μ A; in that range, u_h is nearly constant and about -7.

4 Monte Carlo models

Even if computationally much more intensive than previous fluid models, PIC-MC (Particle In Cell-Monte Carlo) simulations are the standard choice[5, 16] because they are simpler to define and they naturally follow the time evolution of the system; in particular they verify whether SCC stationary equilibrium is stable or not. For this reasons, we also develop a MC tool: starting from an assigned space charge distribution n_a^0, the electric field is computed by the Comsol Multiphysics solver for Poisson equation. Then new particles are generated continuously according to eq. 1; new particles (and the old ones if any) are advanced with a leap-frog method for a given number N_s (typically 1) of time steps $\mathrm{d}t$. After, space charge is updated, Poisson equation is solved again, and time evolution is resumed. Also the H^- beam trajectories can be updated after a longer period $\mathrm{d}t_2$, with a call to the 'postplot' routine of Comsol Multiphysics.

The particles involved have quite different velocities, that is, v_b for H^- and $v_2 = (2T_g/m_{H_2^+})^{1/2}$ with $T_g = 0.025$ eV the gas temperature at start; similarly $v_e = (2T_e/m_e)^{1/2}$ for electrons with $T_e = 10$ eV. We get $v_e \cong 10^6$ m/s and $v_2 \cong 10^3$ m/s.

To follow the dynamics of the whole systems we should choose the characteristic time step $\mathrm{d}t$ of our simulation. So, according to electron velocity and Debye length we obtain $\mathrm{d}t = \lambda_D/v_e \cong 1.7 \times 10^{-10}$ s; scaling to a lower density beam $n_b = 10^{13}$ m^{-3}, we can use $\mathrm{d}t = 10^{-9}$ s.

The secondary production is

$$R_s = \mathrm{d}\,N_2/\,\mathrm{d}t = N_g N_0 n_b(x)\sigma_1 \qquad (14)$$

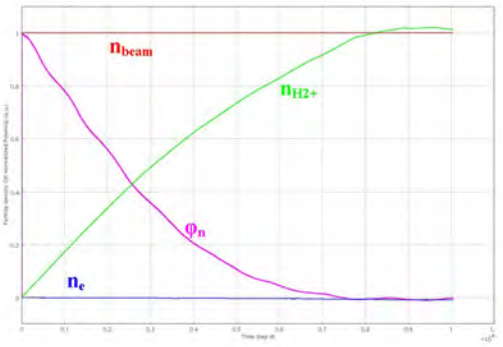

Figure 9: Evolution of $\phi(t)/\phi(t=0)$ at central axis point $z = L_z/2$, and of normalized particles densities vs time index $t/\,\mathrm{d}t$.

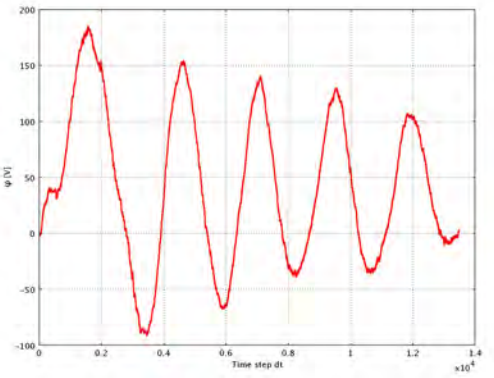

Figure 10: Potential well depth $\phi(L_z/2, 0)$ vs time index $t/\,\mathrm{d}t$

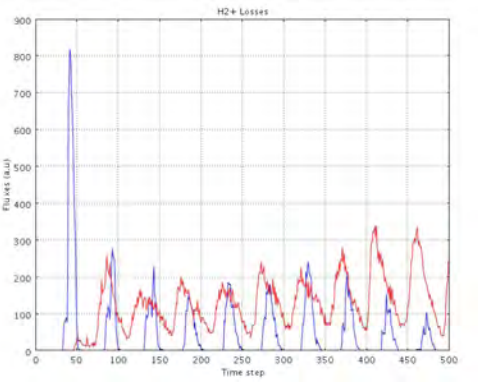

Figure 11: Flux oh H_2^+ leaving the domain vs time. Red line: radial flux, Blue line: axial flux. Electrons behavior is similar.

So that an effective density of secondary $n_s = R_s\,\mathrm{d}t$ is created at each time step, and divided into an suitable number of macroparticles whose positions are chosen randomly inside the beam region with a velocity depending on particles species.

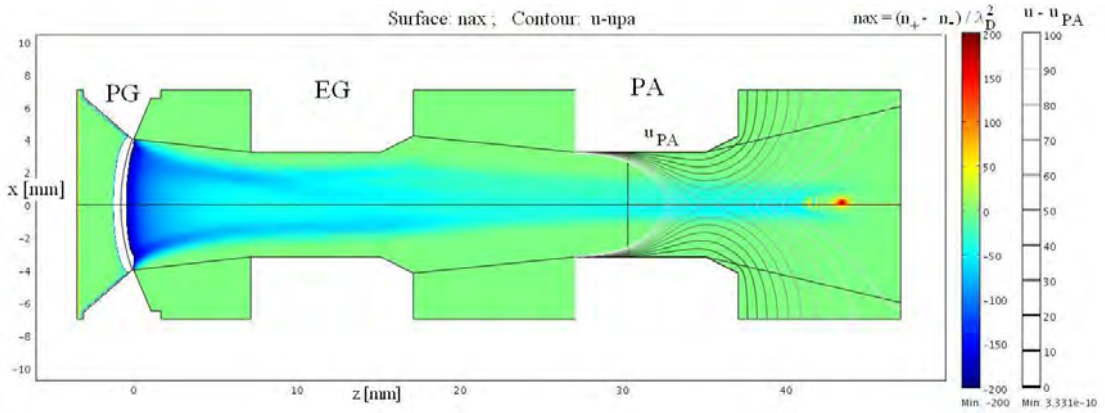

Figure 12: The selfconsistent total space charge n_{ax} from BYPO: note that H^- beam (blue or azure) merges into the green area (net charge 0) after the red spot; some equipotential near the postacceleration electrode PA are also shown

4.1 Monte Carlo results

The drift length $L_z = 0.5$ m is longer than in the fluid simulations and the PA hole region is omitted, setting $u_1 = 0$ in eq 11. Lateral boundary conditions are as for a single beamlet, that is, eq 10.

In a first series of simulation, secondary charge was zero at start, that is $n_a^0 = -n_b$; this give a huge potential well (negative for potential ϕ) so that beam opens up at a first time until SCC is enough to significantly reduce this potential well; after that beam can propagate with minor perturbation.

Beam reflection was also observed with dense beam. Due to the many time scales involved, some time oscillation may appear (and eventually damp): generally, ion losses oscillate between axial and radial directions; electron losses roughly have the opposite phase.

The potential is expected to have a maximum depth at the central point $z = L_z/2$ and $x = 0$; let ϕ_R be the ratio of this potential depth and its value at $t = 0$. Figure 9 shows time evolution of ϕ_R and of the normalized particle densities. This depth is drastically reduced by the accumulation of H_2^+ ions, and the neutralization is reached in a time $\tau_n = 9{\times}10^{-9}$ s close to the theoretical SCC time defined as $\tau = 1/(\sigma_1 * N_g * v_b) = 6.3{\times}10^{-9}$ s. Electron apparently do not play a role in the transient phase of compensation, since they are fastly expelled from the beam.

In a second series of simulations, to better analyze whether the SCC is stable or not, the transient phase of the SCC was shortened by starting with a neutralization degree of 99.9% . Picture 10 shows the value of the potential depth $\phi(L_z/2, 0)$. An oscillating potential is found, reflecting the way the beams adjust for maintaining its degree of neutralization: secondaries are expelled or accumulated depending on their charge and the potential oscillates between the points of maximum accumulation of both species. Compared to the beam accelerating voltages of 100 kV the amplitudes of these oscillations are relatively small, and tend to decrease in time; their effect on beam optic is negligible and the SCC appear basically stable. Picture 10 shows the fluxes of H_2^+ ions expelled from the beam and leaving the domain in the axial or radial direction. Obviously the two quantities are correlated on beam potential: ions leaves the domain radially especially during the H_2^+ accumulating phase ($\phi < 0$) while, when potential becomes positive they are expelled axially, gaining an acceleration proportional to potential . Electrons follow a similar dynamics with oppoaite phase. So, in spite of the qualitative results of this simulation, an important topic was pointed out thanks to the 2D geometry: due to the fact that the radial potential is very small compared to the axial one, particles are expelled from the beam in all directions, meaning the dynamic of the phenomena is not simply radial, as previously supposed.

5 Comparison with Bypo

An important new feature of the code BYPO which addresses the whole 2D geometry of

the accelerator column was a model for the SCC (see figure 12); anyway the simulated span of the drift region is rather short (2 cm). For this reason an ad hoc model, tunable to follow results of more detailed models, was inserted into BYPO. In current notation

$$n_2 = R_2^{sc}\,\Theta(u_{,z})\mathrm{e}^{(u-u_h)/T_2} \qquad (15)$$
$$n_e = R_e^{sc}\;\; 2/(1+\mathrm{e}^{(u-u_h)/T_e})$$

where end potential u_h is iteratively adjusted from BYPO, R_2^{sc} and R_e^{sc} are the assigned fraction of density of H_2^+ and electrons at point $(z_h, 0)$ with respect to average beam density as computed by a 1D analytical model[4]. In our case $R_2^{sc} = 0.9986$ and $R_e^{sc} = 0.0023$. Similarly T_2 and T_e are the assigned ion and electron temperature (divided by T_0); here $T_e = 12.0$ from that analytic model[4] and $T_2 = 0.8$ as an user guess. For H_2^+ a maxwellian distribution was used, which is not invalid where ions are confined; indeed the Heaviside function Θ has the purpose to limit n_2 to region where the ion are axially confined. This agrees to intuitive expectations and as saw it is not exactly confirmed by our 2D model.

It should be noted that even if equipotential found are in reasonable agreement with the model section 2 and 3, BYPO space charge looks correct only on the average, with some fluctuation apparent. The advantage of more detail diffusive model over simpler local model like eq. 15 is thus evident.

References

[1] A. BenIsmail et al, Space charge compensation studies of hydrogen ion beams in a drift section Phys. Rev. ST-AB 10, 070101 (2007)

[2] M. Cavenago, P. Veltri, F. Sattin, G. Serianni, V. Antoni, *IEEE Trans. on Plasma Science*, **36**, pp 1581-1588 (2008)

[3] M. Cavenago, P. Veltri, N. Pilan, P. Antonini, Simulations of Negative Ion Beams and Sources, in Comsol 2008 User Conference, CD-ROM (2008)

[4] A. T. Holmes, *Beam Transport*, in *The Physics and Technology of Ion Sources*, (ed. I.G. Brown), J. Wiley, NY, 1989

[5] N. Chauvin et al., Proceedings of LINAC08, Victoria, BC, Canada, 242

[6] I. A. Soloshenko, Transportation of intensive ion beams, Rev. Sci. Instrum. **69**, 1359 (1998)

[7] `http://www-amdis.iaea.org/ALADDIN` and links

[8] H. P. L. de Esch, R. S. Hemsworth, and P. Massmann, SINGAP: The European concept for negative ion acceleration in the ITER neutral injectors, Rev. Sci. Instrum., **73**, pp1045-1047 (2002)

[9] T. Inoue et al., "Design of neutral beam system for ITER-FEAT", Fus. Eng. and Design 56-57 (2001) 517-521

[10] P. Agostinetti et al., "Design of a low voltage, high current extraction system for the ITER Ion Source" , in *Negative Ions Beams and Sources, 1st Int. Symposium*, AIP CP **1097**, (ed. E. Surrey, A. Simonin, AIP, Melville, 2009), p. 325

[11] R. N. Franklin, The plasma-sheath boundary region, J. Phys. D: Appl. Phys. 36 (2003) R309-R320

[12] R. K. Janev, D. Reiter, and U. Samm, Collision processes in low-temperature hydrogen plasmas, Tech. Rep. Jul-4105, Forschungszentrum Julich (2003)

[13] K. Miyamoto, *Plasma Physics for nuclear fusion*, The MIT Press, Cambridge (1976)

[14] T.J.R. Hughes, T.E. Tezduyar, Comput. Methods Appl. Mech. Engrg. **45**, 217-284 (1984).

[15] Comsol MultiPhysics 4.0 documentation, CFD Module UserGuide, Theory for the Laminar Flow Interface (2009)

[16] G. Fubiani, H. P. L. de Esch, A. Simonin, R. Hemsworth, Phys. Rev. ST-AB, **11**, 014202 (2008)

[17] M.Cavenago, "Structures of Charge Sheaths and Transition Layers in Ion Sources", in "Collective Phenomena in Macroscopic Systems " (eds. G Bertin, R Pozzoli, M Rom , K R Sreenivasan, World Scientific, Singapore), pp 225-230 (2007)